Anomalous modulation of a zero bias peak in a hybrid nanowire-superconductor device

A.D.K. Finck[1], D.J. Van Harlingen[1], P.K. Mohseni[2], K. Jung[2], X. Li[2]
[1]*Department of Physics and Materials Research Laboratory, University of Illinois at Urbana-Champaign, Urbana, Illinois 61801*
[2]*Department of Electrical and Computer Engineering, Micro and Nanotechnology Laboratory, University of Illinois at Urbana-Champaign, Urbana, Illinois 61801*
(Dated: December 27, 2012)

We report on sub-gap transport measurements of an InAs nanowire coupled to niobium nitride leads at high magnetic fields. We observe a zero-bias anomaly (ZBA) in the differential conductance of the nanowire for certain ranges of magnetic field and chemical potential. The ZBA can oscillate in width with either magnetic field or chemical potential; it can even split and reform. We discuss how our results relate to recent predictions of hybridizing Majorana fermions in semiconducting nanowires, while considering more mundane explanations.

PACS numbers: 71.10.Pm, 73.63.Nm, 74.45.+c, 74.78.Na

Majorana fermions are neutral particles that are their own antiparticles. Although they were first proposed to describe fundamental particles such as neutrinos [1], recent years have seen intense interest in realizing solid state systems with quasi-particles that behave like MFs [2, 3]. There are several candidates, ranging from certain quantum Hall states [4] to topological insulators coupled with s-wave superconductors [5]. Once their presence is confirmed, MFs can be used to create a fault-tolerant topological quantum computer, in which the non-Abelian exchange statistics of the MFs are used to process quantum information non-locally, evading error-inducing local perturbations [6, 7].

A conceptually simple realization of MFs employs a one-dimensional spinless p-wave superconductor [8]. One can engineer this system in a semiconductor nanowire with strong spin-orbit coupling that is in contact with a superconductor and exposed to a large magnetic field [9, 10]. This proposal is attractive because supercurrents have already been observed in InAs nanowires [11, 12]. A nanowire with a single occupied subband can be driven through a topological phase transition when $E_Z^2 > \mu^2 + \Delta^2$, where $E_Z = \frac{1}{2} g \mu_B B$ is the Zeeman energy, μ is the chemical potential, and Δ is the induced superconducting gap. In the topological phase, the nanowire is predicted to harbor a single pair of MFs. Here, the MFs exist as zero energy modes pinned to the boundaries between two distinct regions of the nanowire: the topological region in which $E_Z^2 > \mu^2 + \Delta^2$ and the trivial region where $E_Z^2 < \mu^2 + \Delta^2$. At the boundary, the single-particle gap collapses and changes sign. Although disorder [13–15], Coulomb interactions [16], and multiple subbands [17–19] might quantitatively change the conditions for MFs, the qualitative picture should remain: for certain ranges of E_Z, μ, and Δ the nanowire will be in the topological regime and contain a pair of MFs.

A key probe for MFs is tunneling spectroscopy [20–24]. The MF would manifest as a peak in the tunneling conductance that is pinned to zero voltage. The MFs can only interact with other MFs, so the peak would stay at zero energy so long as the MFs are spatially separated from each other. Indeed, a number of groups [25–28] have reported zero bias anomalies (ZBAs) in devices inspired by the theoretical proposals. However, it is also recognized that a ZBA might occur under similar conditions due to the appearance of a Kondo resonance that manifests when the magnetic field has suppressed the superconducting gap enough to permit the screening of a localized spin [29]. Thus, it is necessary to seek more definitive signatures of MFs.

One possibility is to look for signs that the MFs are hybridizing with each other [30–35]. Because the wave functions of MFs decay exponentially within the interior of the topological nanowire, MFs at the ends of a nanowire with finite length will overlap with each other and hybridize to some degree. The amount of hybridization can be tuned by the Zeeman energy or chemical potential, which would alter the decay length of the MF wave function as well as the period of its oscillatory component. The ZBA would then split and reform in a periodic fashion, in contrast with the linear splitting expected for the Kondo effect.

In this Letter, we report on the behavior of ZBAs in an InAs nanowire coupled to superconducting leads. We focus on the regime of large magnetic fields, which are thought to suppress extraneous effects such as Josephson supercurrents, Kondo resonances [36, 37], and reflectionless tunneling [38]. We find that the ZBAs are robust against changes in Zeeman energy and chemical potential, as expected for MFs. Under certain conditions, the width of the ZBA oscillates with either parameter. The ZBA can even split and reform. While some of this behavior may be explained by resonant level effects, certain modulations of the ZBA require alternative explanations and new physics.

Metal-organic chemical vapor deposition growth of

InAs nanowires with 100 nm diameters was performed using the Au-assisted vapor-liquid-solid approach, while simultaneously flowing disilane to achieve *in situ* doping. TEM analysis reveals a nearly purely hexagonal (wurtzite) crystal structure, with only a few stacking faults near the nanowire tips. The nanowires are then deposited on a highly doped Si substrate with a 300 nm thick SiO_2 dielectric, permitting back gating. We optically locate the nanowires with respect to alignment marks. Superconducting leads are defined by conventional e-beam lithography. The leads overlapping the nanowire are each 1 μm wide and separated by approximately 150 nm. We sputter 55 nm of niobium nitride via a DC sputter gun and a Nb target in an Ar environment with a partial pressure of N_2. Immediately prior to sputtering, the contact regions are briefly exposed to an Ar ion mill, which etches away the native oxide and permits transparent contacts [39]. We note that the ion milling likely raises the carrier density within the contact region with respect to the unetched InAs nanowire [40]. The NbN thin film has a critical temperature of 12 K and an upper critical field of 9 T at 10 K. The sample is lowered into the mixing chamber of a top-loading He-3/He-4 dilution refrigerator. Immersion in the dilute phase of the mixture provides an excellent thermal sink for the nanowire as evidenced by the continuing evolution of the transport measurements below 50 mK. The I-V characteristics of the superconductor/nanowire/superconductor junction are measured via standard lockin techniques, employing a 10 μV AC excitation at 73 Hz. Unless otherwise stated, all data reported here were taken at a mixing chamber temperature of 10 mK.

To demonstrate that a superconducting proximity effect is induced in the nanowire, we first consider the transport properties of the nanowire while passing current between the two superconducting leads at zero magnetic field. We focus on the regime when the nanowire supports a small number of open channels and has a normal state conductance of $\sim e^2/h$. Two representative conductance curves are shown in Figure 1b. Here, we observe an enhancement of the differential conductance for source-drain voltage $|V_{SD}| < 4$ mV by a factor of 2 beyond the conductance achieved at high V_{SD}. Our NbN thin films generally have a gap of $\Delta_0 \approx 2$ meV, suggesting that we are observing Andreev reflection at the transparent nanowire-superconductor interface for $|V_{SD}| < 2\Delta_0$ [41], with an additional voltage drop across the bare portion of the nanowire.

For the regime of moderate back gate bias, the conductance near $V_{SD} = 0$ fluctuates between having either a valley or peak shape superimposed on the background Andreev reflection plateau with periodicity of $\Delta V_{BG} \approx 0.6$ V. The maximum width of each valley or peak regularly occurs at $|V_{SD}| = 600$ μV for a wide range of density. Coherence peaks can also be discerned at this voltage for certain ranges of V_{BG}. The periodic behavior of the valleys and peaks is likely caused by resonant levels within the bare nanowire segment passing through zero energy and allowing transport between the proximitized nanowire segments [42]. This is verified by the presence of a checkerboard pattern in the stability diagram that becomes more apparent beyond $V_{BG} = 12$ V, the characteristic of resonant levels tuned by the back gate [43–45]. We tentatively identify the energy scale 600 μV with twice the induced gap of the proximitized nanowire segments [46], 2Δ. When the transmission probability through the bare nanowire segment is low, we observe suppressed conductance for energies below the induced gap of the adjacent nanowire segments. Otherwise, we observe Andreev reflection in this energy range.

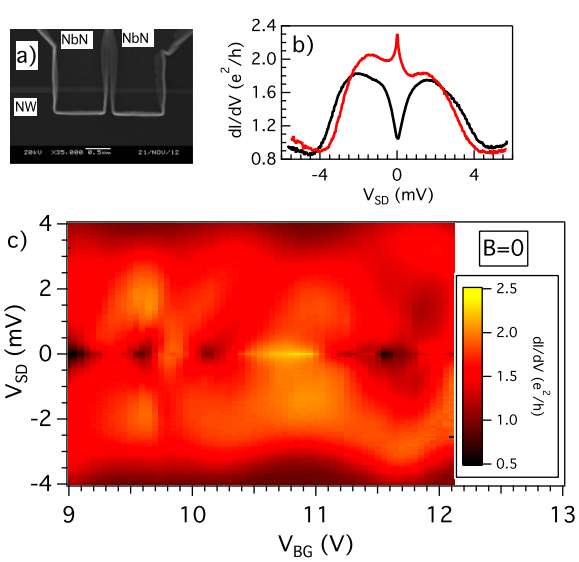

FIG. 1: (a) SEM image of NbN leads on InAs nanowire (NW). The white feature at the edges of the NbN leads is PMMA residue from the ion milling. (b) Transport at $B = 0$ for $V_{BG} = 10.1$ V (black) and 10.9 V (red). (c) Stability diagram at $B = 0$ for region of interest.

At $B = 0$, we see no true DC supercurrent but we do observe a number of sharp peaks at zero bias that become less prevalent beyond $V_{BG} = 15$ V. As V_{BG} changes, the peaks split and evolve into sharp dips, suggesting a complex interplay between superconductivity and the Kondo effect [29, 47–52]. In the case of $V_{BG} = 10.9$ V, a zero bias peak in conductance is visible, which disappears without signs of splitting beyond $B = 0.4$ T, comparable to the estimated 0.14 T required to have one magnetic flux quantum through the nanowire section between the superconducting leads. This suggests that the peak results from phase-coherent transport through the nanowire that is broadened by noise or thermal fluctuations. The peak's critical field is consistent with other Josephson junctions based on semiconducting nanowires with similar dimensions and niobium leads [12, 53]. Thus, we can conclude that phase-coherent transport across the

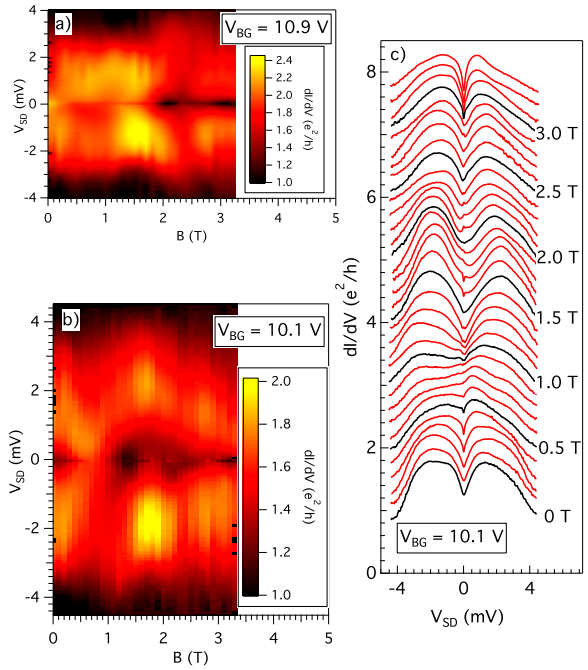

FIG. 2: (a) and (b) Conductance traces vs magnetic field for two different densities. (c) Individual traces for $V_{BG} = 10.1$ V, each trace differing by 0.1 T. Adjacent curves are offset for clarity.

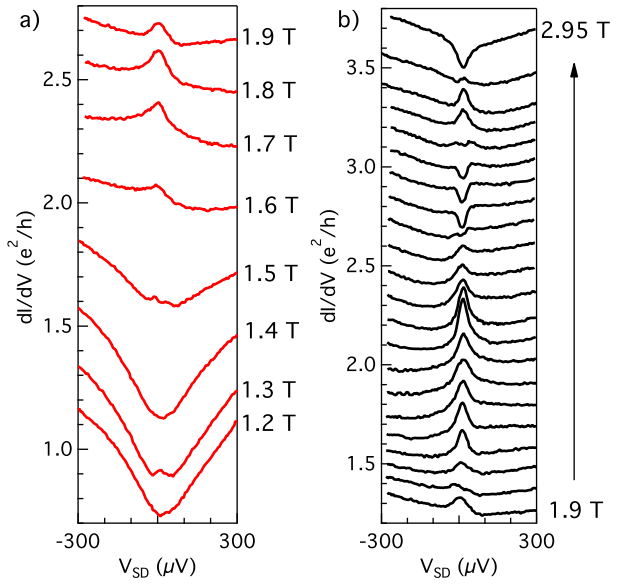

FIG. 3: (a) and (b) Conductance traces at $V_{BG} = 10.1$ V for various B values. In (b), the traces differ by $\Delta B = 0.05$ T. Adjacent curves are offset for clarity.

exposed nanowire section is likely to be highly suppressed for $B > 0.4$ T.

We now consider transport when a large magnetic field is applied perpendicular to the Si substrate. In Figure 2 we show color plots of dI/dV vs V_{SD} and B at two different densities. For $V_{BG} = 10.9$ V, one can observe the zero bias peak at $B = 0$ disappear quickly. Note that the enhancement of conductance for $V_{SD} < 2\Delta_0$ is still present up to $B = 3.2$ T, verifying the persistence of the proximity effect. However, there is no evidence for a ZBA at this density beyond $B = 0.4$ T.

The situation is dramatically different for $V_{BG} = 10.1$ V. At this density, the proximity gap seems to close at $B \approx 0.8$ T. Exceeding this field, the gap reopens and then gradually closes with increasing field. Beyond $B = 0.8$ T, a number of ZBAs are visible. We repeated the measurement in higher resolution to see the detailed evolution of the ZBA, shown in Figure 3. The ZBA persists for a range of magnetic field values, sometimes more than 100 mT. The ZBA periodically splits and reforms, with a characteristic interval of $\Delta B \approx 0.6$ T. A slight disagreement on the location of the ZBA between Figure 2c and Figure 3 is likely due to charge noise.

At this point it is tempting to attribute the ZBA to the presence of MFs within the nanowire. In this picture, the magnetic field drives portions of the nanowire through a topological phase transition when the Zeeman energy is sufficiently large. The critical field for this transition is a function of chemical potential, thus explaining why no such ZBAs are present at a higher density and why we also observe the gap close at lower field ($B = 0.6$ T) at an even lower density ($V_{BG} = 9.35$ V). While in the topological phase, segments of the nanowire can support zero energy end modes. For example, the regions of the nanowire in direct contact with the NbN leads could exist in the topological regime for certain magnetic field values while the bare nanowire segment, possessing a weaker induced gap, is in the trivial regime. The MFs at the boundaries between the topological and nontopological segments could then allow the passage of single charges through the bare nanowire segment at zero energy. Without the MFs, transport through the nanowire is suppressed near zero bias by the superconducting gap, as demonstrated in Figure 2a.

In this interpretation, the periodic splitting of the ZBA would be naturally explained by the hybridization of the MFs. The Zeeman energy would tune the overlap of the MF wave functions in a periodic fashion, leading to a oscillatory splitting of the ZBA. For example, Ref. [35] calculates the period of this splitting to be $\Delta E_Z = 0.2$ meV for a 1 μm long topological wire segment. Determining the Zeeman energy for real devices is difficult due to complications such as confinement [54] and the role of spin-orbit coupling, both of which can be tuned by external fields [55–57]. Simply assuming a value of $g = 20$ gives a measured period of $\Delta E_Z = 0.35$ meV, in rough agreement with Ref. [35].

To further test the case for MFs in our nanowire device, we explore the behavior of the ZBA with respect

to changes in chemical potential. In Figure 4a, we show plots of dI/dV vs source-drain voltage V_{SD} and back gate voltage V_{BG} for $B = 2.3$ T. A ZBA is visible for two different ranges of gate bias. The persistence of the ZBA with chemical potential is suggestive of a stable set of MFs; their periodic appearance and disappearance would then indicate the gate-tuned hybridization of the MFs. However, a careful inspection of Figure 4a reveals a subtle checkerboard pattern for $|V_{SD}| < 0.7$ meV. The separation in back gate bias for this pattern is $\Delta V_{BG} = 0.4$ V, comparable to the periodicity observed at $B = 0$. We posit that this pattern comes from the quantized energy levels resulting from partial confinement of electrons in the exposed nanowire, also visible at $B = 0$. These levels are broadened due to finite coupling to adjacent segments, giving the appearance of broad features in the stability diagram as well as persistent ZBAs. By crossing at zero energy, these energy levels provide the necessary degeneracy to create a ZBA through a form of the Kondo effect. Indeed, the temperature dependence of the height of the ZBA in this regime is consistent with a Kondo effect with a Kondo temperature $T_K \approx 970$ mK [37, 58], as shown in Figure 5. The resonant levels also evolve with magnetic field; thus the periodic crossing of these levels would explain the modulation of the ZBA in Figure 2b. It is not clear why neither crossings nor ZBAs are apparent at $V_{BG} = 10.9$ V, as shown in Figure 2a.

As a final note, we also see modulations of the ZBA with frequencies that do not fit a simple picture of regularly crossing resonant levels. For example, in Figure 4b we show a ZBA that repeatedly splits and reforms in the range of $V_{BG} = 10$ V to 10.7 V, with a period of $\Delta V_{BG} \approx 0.175$ V. In the Supplementary Material, we show a ZBA whose width fluctuates with a period of $\Delta V_{BG} = 0.1$ V. Curiously, this ZBA becomes steadily narrower as the temperature increases, disappearing beyond T = 700 mK. The identity of these oscillations is an open question.

In conclusion, we observe a series of pronounced ZBAs in a nanowire-superconductor device at high magnetic fields. Their periodic splitting and reforming are in qualitative and quantitative agreement with hybridizing MFs, whose wave function overlap is governed by Zeeman energy and chemical potential. However, we also find evidence that this behavior is caused by confined states crossing zero energy and generating a Kondo resonance. Our results indicate that spectroscopic studies of hybridizing MFs should be interpreted with caution.

We gratefully acknowledge technical assistance from C. English, C. Kurter, C. Nugroho, V. Orlyanchik, and M. Stehno. We have benefited from conversations with W. DeGottardi, B. Dellabetta, S. Frolov, P. Ghaemi, M. Gilbert, T. Hughes, V. Manucharyan, D. Rainis, and S. Vishveshwara. A.D.K.F. and D.J.V.H. acknowledge funding by Microsoft Project Q. P.K.M., K.J., and X.L. acknowledge funding from NSF DMR under Award Number 1006581. Device fabrication was carried out in the MRL Central Facilities (partially supported by the DOE under DE-FG02-07ER46453 and DE-FG02-07ER46471).

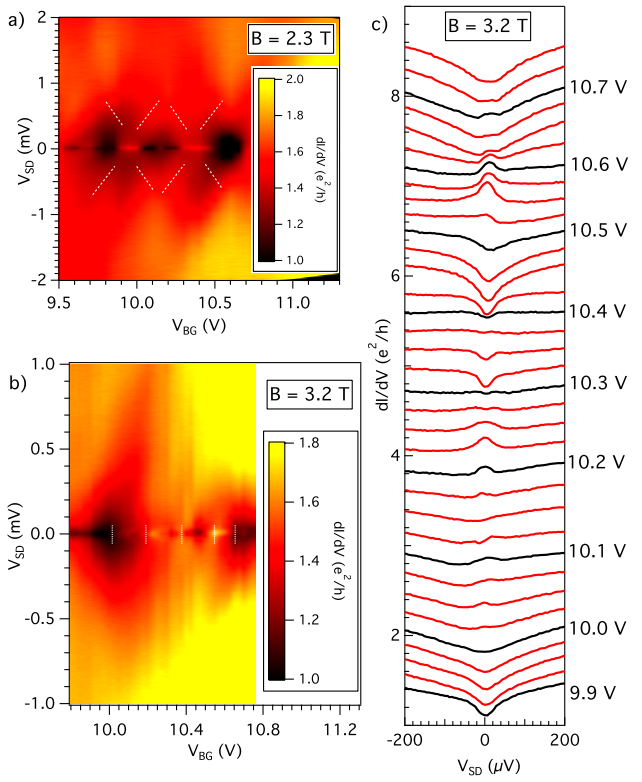

FIG. 4: Stability diagram at (a) $B = 2.3$ T and (b) $B = 3.2$ T. In (a), dashed white lines show location of resonant levels. In (b), dashed white lines delineate individual periods of ZBA oscillations. (c) Individual traces for $B = 3.2$ T in steps of $\Delta V_{BG} = 0.025$, with adjacent curves offset for clarity.

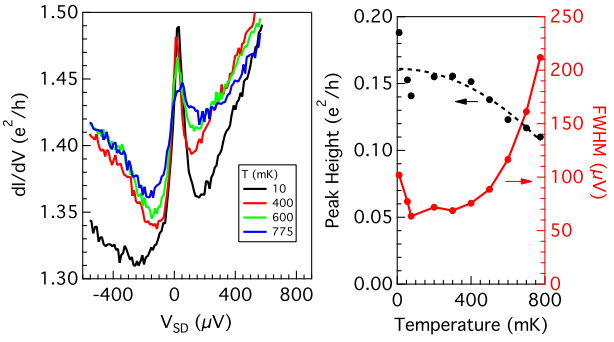

FIG. 5: (a) ZBA temperature dependence at $B = 2.75$ T and $V_{BG} = 10.35$ V. (b) Peak height (black) and FWHM (red) vs T, after subtracting off background. Black dashed line is parabolic fit based on Ref. [37] with $T_K = 970$ mK.

[1] E. Majorana, Nuovo Cimento **14**, 171 (1937).
[2] C. Beenakker, arXiv:1112.1950 (2011).
[3] J. Alicea, Rep. Prog. Phys. **75**, 076501 (2012).
[4] N. Read and D. Green, Phys. Rev. B **61**, 10267 (2000).
[5] L. Fu and C. L. Kane, Phys. Rev. Lett. **100**, 096407 (2008).
[6] S. Das Sarma, M. Freedman, and C. Nayak, Phys. Rev. Lett. **94**, 166802 (2005).
[7] C. Nayak, S. H. Simon, A. Stern, M. Freedman, and S. Das Sarma, Rev. Mod. Phys. **80**, 1083 (2008).
[8] A. Kitaev, Phys.-Usp. **44**, 131 (2001).
[9] R. M. Lutchyn, J. D. Sau, and S. Das Sarma, Phys. Rev. Lett. **105**, 077001 (2010).
[10] Y. Oreg, G. Refael, and F. von Oppen, Phys. Rev. Lett. **105**, 177002 (2010).
[11] Y.-J. Doh, J. A. van Dam, A. L. Roest, E. P. A. M. Bakkers, L. P. Kouwenhoven, and S. D. Franceschi, Science **309**, 272 (2005).
[12] H. Y. Günel, I. E. Batov, H. Hardtdegen, K. Sladek, A. Winden, K. Weis, G. Panaitov, D. Grützmacher, and T. Schäpers, J. Appl. Phys. **112**, 034316 (2012).
[13] P. W. Brouwer, M. Duckheim, A. Romito, and F. von Oppen, Phys. Rev. B **84**, 144526 (2011).
[14] A. M. Lobos, R. M. Lutchyn, and S. Das Sarma, Phys. Rev. Lett. **109**, 146403 (2012).
[15] L. Fidkowski, R. M. Lutchyn, C. Nayak, and M. P. A. Fisher, Phys. Rev. B **84**, 195436 (2011).
[16] B. van Heck, F. Hassler, A. R. Akhmerov, and C. W. J. Beenakker, Phys. Rev. B **84**, 180502 (2011).
[17] R. M. Lutchyn, T. D. Stanescu, and S. Das Sarma, Phys. Rev. Lett. **106**, 127001 (2011).
[18] T. D. Stanescu, R. M. Lutchyn, and S. Das Sarma, Phys. Rev. B **84**, 144522 (2011).
[19] R. M. Lutchyn and M. P. A. Fisher, Phys. Rev. B **84**, 214528 (2011).
[20] K. Sengupta, I. Žutić, H.-J. Kwon, V. M. Yakovenko, and S. Das Sarma, Phys. Rev. B **63**, 144531 (2001).
[21] K. T. Law, P. A. Lee, and T. K. Ng, Phys. Rev. Lett. **103**, 237001 (2009).
[22] K. Flensberg, Phys. Rev. B **82**, 180516 (2010).
[23] J. D. Sau, S. Tewari, R. M. Lutchyn, T. D. Stanescu, and S. Das Sarma, Phys. Rev. B **82**, 214509 (2010).
[24] F. Pientka, G. Kells, A. Romito, P. W. Brouwer, and F. von Oppen, Phys. Rev. Lett. **109**, 227006 (2012).
[25] V. Mourik, K. Zuo, S. Frolov, S. Plissard, E. Bakkers, and L. Kouwenhoven, Science **336**, 1003 (2012).
[26] M. T. Deng, C. L. Yu, G. Y. Huang, M. Larsson, P. Caroff, and H. Q. Xu, Nano Letters **12**, 6414 (2012).
[27] A. Das, Y. Ronen, Y. Most, Y. Oreg, M. Heiblum, and H. Shtrikman, Nature Phys. **8**, 887 (2012).
[28] W. Chang, V. Manucharyan, T. Jespersen, J. Nygard, and C. Marcus, arXiv:1211.3954 (2012).
[29] E. J. H. Lee, X. Jiang, R. Aguado, G. Katsaros, C. M. Lieber, and S. De Franceschi, Phys. Rev. Lett. **109**, 186802 (2012).
[30] M. Cheng, R. M. Lutchyn, V. Galitski, and S. Das Sarma, Phys. Rev. Lett. **103**, 107001 (2009).
[31] M. Cheng, R. M. Lutchyn, V. Galitski, and S. Das Sarma, Phys. Rev. B **82**, 094504 (2010).
[32] D. Pikulin and Y. Nazarov, JETP Lett. **94**, 693 (2011).
[33] E. Prada, P. San-Jose, and R. Aguado, Phys. Rev. B **86**, 180503 (2012).
[34] D. Rainis, L. Trifunovic, J. Klinovaja, and D. Loss, arXiv:1207.5907 (2012).
[35] S. Das Sarma, J. D. Sau, and T. D. Stanescu, Phys. Rev. B **86**, 220506 (2012).
[36] D. Goldhaber-Gordon, H. Shtrikman, D. Mahalu, D. Abusch-Magder, U. Meirav, and M. A. Kastner, Nature **391**, 156 (1998).
[37] A. V. Kretinin, H. Shtrikman, D. Goldhaber-Gordon, M. Hanl, A. Weichselbaum, J. von Delft, T. Costi, and D. Mahalu, Phys. Rev. B **84**, 245316 (2011).
[38] B. J. van Wees, P. de Vries, P. Magnée, and T. M. Klapwijk, Phys. Rev. Lett. **69**, 510 (1992).
[39] T. Nishio, T. Kozakai, S. Amaha, M. Larsson, H. A. Nilsson, H. Xu, G. Zhang, K. Tateno, H. Takayanagi, and K. Ishibashi, Nanotechnology **22**, 445701 (2011).
[40] P. Magnée, S. den Hartog, B. van Wees, T. Klapwij, W. van de Graaf, and G. Borghs, Appl. Phys. Lett. **67**, 3569 (1995).
[41] G. E. Blonder, M. Tinkham, and T. M. Klapwijk, Phys. Rev. B **25**, 4515 (1982).
[42] M. R. Buitelaar, W. Belzig, T. Nussbaumer, B. Babić, C. Bruder, and C. Schönenberger, Phys. Rev. Lett. **91**, 057005 (2003).
[43] P. Jarillo-Herrero, J. van Dam, and L. Kouwenhoven, Nature **439**, 953 (2006).
[44] H. I. Jørgensen, K. Grove-Rasmussen, T. Novotný, K. Flensberg, and P. E. Lindelof, Phys. Rev. Lett. **96**, 207003 (2006).
[45] A. V. Kretinin, R. Popovitz-Biro, D. Mahalu, and H. Shtrikman, Nano Letters **10**, 3439 (2010).
[46] F. Deon, V. Pellegrini, F. Giazotto, G. Biasiol, L. Sorba, and F. Beltram, Phys. Rev. B **84**, 100506 (2011).
[47] A. F. Morpurgo, J. Kong, C. M. Marcus, and H. Dai, Science **286**, 263 (1999).
[48] M. R. Buitelaar, T. Nussbaumer, and C. Schönenberger, Phys. Rev. Lett. **89**, 256801 (2002).
[49] A. Eichler, M. Weiss, S. Oberholzer, C. Schönenberger, A. Levy Yeyati, J. C. Cuevas, and A. Martín-Rodero, Phys. Rev. Lett. **99**, 126602 (2007).
[50] C. Buizert, A. Oiwa, K. Shibata, K. Hirakawa, and S. Tarucha, Phys. Rev. Lett. **99**, 136806 (2007).
[51] A. Eichler, R. Deblock, M. Weiss, C. Karrasch, V. Meden, C. Schönenberger, and H. Bouchiat, Phys. Rev. B **79**, 161407 (2009).
[52] Y. Kanai, R. S. Deacon, A. Oiwa, K. Yoshida, K. Shibata, K. Hirakawa, and S. Tarucha, Phys. Rev. B **82**, 054512 (2010).
[53] R. Frielinghaus, I. E. Batov, M. Weides, H. Kohlstedt, R. Calarco, and T. Schäpers, Appl. Phys. Lett. **96**, 132504 (2010).
[54] A. A. Kiselev, E. L. Ivchenko, and U. Rössler, Phys. Rev. B **58**, 16353 (1998).
[55] S. Csonka, L. Hofstetter, F. Freitag, S. Oberholzer, C. Schonenberger, T. S. Jespersen, M. Aagesen, and J. Nygrd, Nano Letters **8**, 3932 (2008).
[56] H. A. Nilsson, P. Caroff, C. Thelander, M. Larsson, J. B. Wagner, L.-E. Wernersson, L. Samuelson, and H. Q. Xu, Nano Letters **9**, 3151 (2009).
[57] M. D. Schroer, K. D. Petersson, M. Jung, and J. R. Petta, Phys. Rev. Lett. **107**, 176811 (2011).
[58] D. Goldhaber-Gordon, J. Göres, M. A. Kastner, H. Shtrikman, D. Mahalu, and U. Meirav, Phys. Rev. Lett. **81**, 5225 (1998).

Supplementary Materials: Anomalous modulation of a zero bias peak in a hybrid nanowire-superconductor device

A.D.K. Finck[1], D.J. Van Harlingen[1], P.K. Mohseni[2], K. Jung[2], X. Li[2]
[1]*Department of Physics and Materials Research Laboratory, University of Illinois at Urbana-Champaign, Urbana, Illinois 61801*
[2]*Department of Electrical and Computer Engineering, Micro and Nanotechnology Laboratory, University of Illinois at Urbana-Champaign, Urbana, Illinois 61801*
(Dated: December 27, 2012)

PACS numbers: 71.10.Pm, 73.63.Nm, 74.45.+c, 74.78.Na

NANOWIRE GROWTH

Metal-organic chemical vapor deposition (MOCVD) growth of InAs nanowires (NWs) was performed using a horizontal-flow, low-pressure reactor (AIXTRON 200/4), through the Au-assisted vapor-liquid-solid (VLS) approach. Pre-growth sample preparation of InAs (110) substrates involved a surface degreasing process with standard solvents and native-oxide etching in a dilute hydrochloric acid (HCl) solution, followed by a poly-L-lysine surface coating procedure and substrate decoration with 50 nm Au colloids. Trimethyl-indium (TMI, $(CH_3)_3In$) and arsine (AsH_3) were employed as sources for the supply of group-III and group-V growth species, respectively, at a constant V/III ratio of 9.8. Nanowire growths were initiated at a reaction temperature of 450 °C, under a constant 5 L/min flow of hydrogen (H_2) carrier-gas, at a system pressure of 200 mBar. In-situ Si doping of InAs NWs was provided through the supply of disilane (Si_2H_6), in tandem with the flow of TMI. Nanowire growths were terminated, after a period of 15 minutes, through the simultaneous cessation of TMI and disilane flows. Samples were permitted to cool from the growth temperature under a constant supply of AsH_3. Transmission electron microcscopy (TEM) experiments revealed that InAs NWs grown under these conditions exhibit a purely hexagonal (wurtzite) crystal structure, with only several monolayers of zincblende crystal growth at the NW tip. The cubic-phase found at NW tips is attributed to the so-called "cooling neck" phenomenon [1, 2].

SUPPRESSION OF SUPERCURRENT PEAK WITH MAGNETIC FIELD

In Figure S1 we show the zero bias conductance vs magnetic field for $V_{BG} = 10.9$ V and $T = 10$ mK. Under these conditions, a zero bias peak occurs at zero magnetic field and is likely due to a supercurrent subjected to noise from the electromagnetic environment. We see signs of a node near $B = 0.22$ T, close to the expected field (0.14 T) for having a single magnetic flux quantum in the exposed nanowire segment. A second node is visible at twice this value, indicating that two magnetic flux quanta are in the junction. Beyond this field, the zero bias peak disappears. For this density, no other ZBA appears up to $B = 3.2$ T.

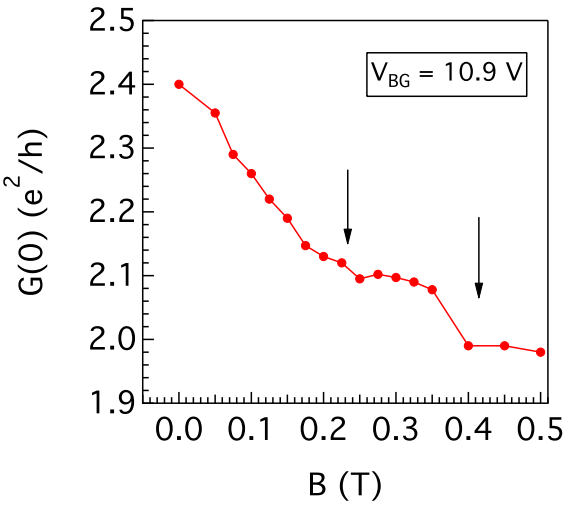

FIG. S1: Zero bias conductance vs magnetic field at $V_{BG} = 10.9$ V and $T = 10$ mK. Arrow indicate presumptive locations of nodes in Fraunhofer diffraction pattern.

ZBA AT LOW DENSITY

In Figure S2a, we show the stability diagram for $B = 2.75$ T. A ZBA can be seen in the region of $V_{BG} = 9.2$ V to 9.7 V. We extract the width of the ZBA by fitting to the data a Lorentzian plus an asymmetric v-shaped background. We plot the FWHM of the fitted Lorentzian vs V_{BG} in Figure S2b. We see clear oscillations in the width with a period of $\Delta V_{BG} \approx 0.1$ V, which does not match with the spacing of the resonant levels within the exposed nanowire segment. In Figure S2c, we show the individual conductance traces.

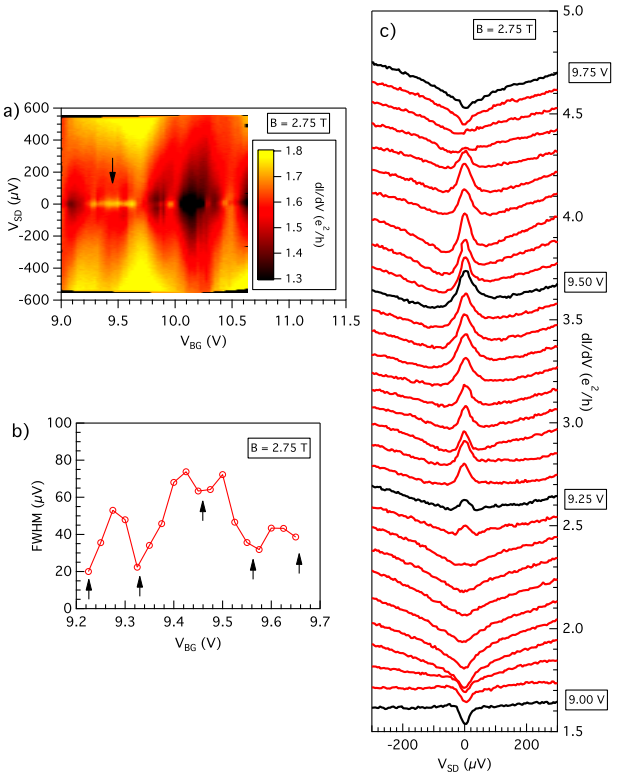

FIG. S2: (a) Stability diagram at $B = 2.75$ T. ZBA is indicated by black arrow. (b) FWHM of ZBA vs V_{BG}. Arrows point at local minima in oscillations. (c) Individual conductance traces for region of interest at $B = 2.75$ T, taken in steps of $\Delta V_{BG} = 0.025$ V. Adjacent curves are offset for clarity.

In Figure S3a, we plot the temperature dependence of the zero-bias anomaly (ZBA) for $V_{BG} = 9.45$ V and $B = 2.75$ T. Once again, we determine the height and width of the ZBA by fitting each curve with a Lorentzian and an asymmetric v-shaped background. Figure S3b shows the height and width of the peak vs temperature. Note that the width seems to decrease with temperature, in contrast to the expected broadening for a Kondo resonance.

[1] Persson, A.I. *et al.* Solid-phase diffusion mechanism for GaAs nanowire growth. Nat. Mater. **3**, 677 (2004).

[2] Plante, M.C. & LaPierre, R.R. Control of GaAs nanowire morphology and crystal structure. Nanotech. **19**, 495603 (2008).

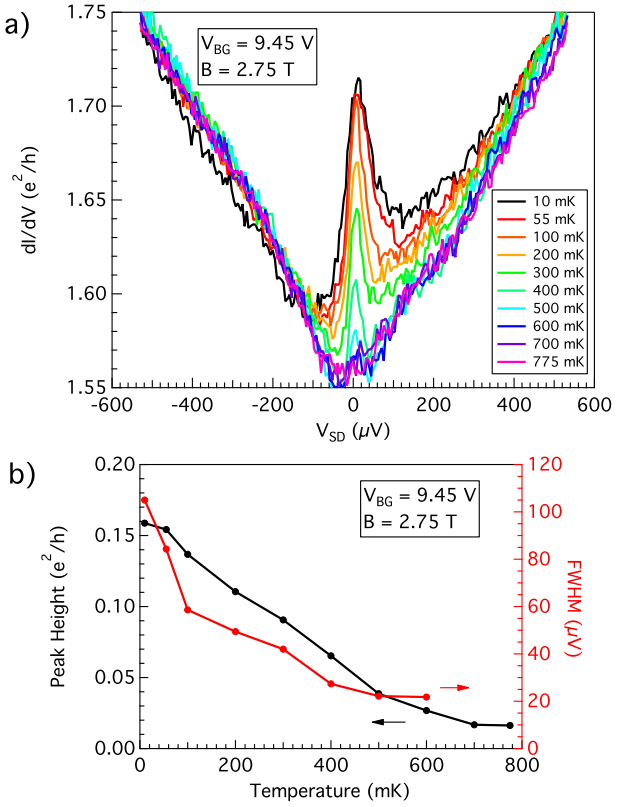

FIG. S3: (a) Temperature dependence of ZBA at $V_{BG} = 9.45$ V and $B = 2.75$ T. (b) Peak height (black trace) and width (red trace) vs temperature.